www.czasopisma.pan.pl PAN www.journals.pan.pl

Opto-Electronics Review 27 (2019) 224–231

Contents lists available at ScienceDirect

Opto-Electronics Review

journal homepage: http://www.journals.elsevier.com/opto-electronics review

Analysis of the beam divergence for one-rod core microstructured optical fibres

D.K. Sharma [a,*], S.M. Tripathi [a,b]

[a] Center for Lasers and Photonics, Indian Institute of Technology Kanpur, Kanpur, 208016, India
[b] Department of Physics, Indian Institute of Technology Kanpur, Kanpur, 208016, India

ARTICLE INFO

Article history:
Received 13 April 2019
Received in revised form 31 May 2019
Accepted 4 June 2019

Keywords:
Marcuse formula
Microstructured optical fibres
Beam divergence
Mode-field diameter
Improved field model

ABSTRACT

The evolution of microstructured optical fibers with hexagonal array (H-MOFs) of air-holes rooted in the background of undoped silica has led to the realization of an ideal host for encouraging and technologically entitled optical properties. We focus to explore the divergence of radiation into free space from the end-facet of solid-core H-MOFs by using the improved theoretical model. Also, we investigated the wavelength dependence of beam divergence angle for principal core mode of H-MOFs under step-index fiber approximation (SIFA). Experimental results have been included for comparison.

1. Introduction

The continuing development of active and passive optical components demands that they would be developed on an ever smaller scale and have to be manipulated on wavelength scale, suggesting the use of available materials in novel ways and developing the material systems with required characteristics [1–4]. One can fabricate new type of optical materials (with previously unattainable optical characteristics) so-called photonic crystal materials [5–7], which are periodically structured dielectric materials in two or three dimensions [1,2] facilitates a strong interaction between the material microstructure and the light. Therefore, such type of materials can significantly enhance the optical performance of the material [2–5]. Photonic crystal materials [6–8] (such as those based on semiconductors [9] and glasses [10]) are the subject of dynamic research due to their potential applications, and provide a platform to tailor the individual characteristics and the promising way of controlling the light [11–14]. One example of the type for such materials is the design of novel fibre (or optical waveguide) with remarkable properties and their potential applications have been explored by several research groups worldwide [15–18]. The first low-loss fibre supporting only a single mode based on 2D photonic crystal materials was demonstrated in the configuration of admirable all-in-silica fibre with hexagonal array of multiple air-holes, known as microstructured optical fibres (H-MOFs) [8]. The H-MOF with one-rod core (i.e., single missing air-hole) permitting low-loss guided wave propagation [12–15] due to their unusual dispersive properties and has been intensively studied during the last few years.

Specific choices of the geometry facilitate two distinct light guiding mechanisms, so-called photonic band gap guidance (PBG) and the effective index guidance, respectively [19,20]. The majority of high-index core MOFs (or holey fibres [21]) have been fabricated from a single material usually pure silica [13,19] but nowadays, active silica MOFs with Yb^{3+} doped cores [22,23] have been developed. Also, MOFs in chalcogenide glasses [24] and in polymers [25] have been fabricated. MOFs have unlatched new opportunities facilitated by high index contrast and wavelength dependent cladding index, for exploring the interaction of light with gases and liquids via evanescent field effects. In addition, they have special geometry which provides long interaction optical path lengths [26,27]. MOFs can be designed to achieve extraordinary optical characteristics such as wide range of single-mode guidance, small mode area for generating nonlinear effects, large mode area for producing high-power beams, and greater controllability in dispersion by altering the air-hole diameter and the pitch (i.e., hole-to-hole spacing) [13–16]. Kim *et al.* [28] have proposed new design parameters for index-guiding MOFs and explored adiabatic mode transformation capability.

One-rod core H-MOF can be compared to equivalent step-index fibre (SIF) with a circular core, and the cladding is assumed to be a homogeneous medium whose effective index is estimated by utilizing the scalar theory [29–32]. The first simplest modelling approach [21] providing useful perception developed for high-index core (or

* Corresponding author.
E-mail addresses: dineshk@iitk.ac.in (D.K. Sharma), smt@iitk.ac.in (S.M. Tripathi).

https://doi.org/10.1016/j.opelre.2019.06.003
1230-3402/

solid-core) MOF was the effective index method [15,29], leading to the definition of *V*-parameter (or normalized frequency) [32]; moreover, it speculates the optical aspects of H-MOF [12–15] distinguishing it from standard SIF [33]. It is noteworthy that weakly guiding approximation [31,34] has been utilized to explore the endlessly single mode guidance [11,13] over an extended wavelength range of H-MOF.

For estimating the coupling efficiency it is vital to have analytical expression for the fundamental mode fields of the two fibres [35–37]. The modal field of SIF can be approximated by a Gaussian function and has been studied extensively for exploring the coupling efficiency [38–41]. Recently, MOFs have been employed in stellar interferometers but due to lack of information regarding the analytical expression for the fundamental mode field, various numerical methods had been adopted [42–45]. Using the Gaussian function merely to approximate MOF's fundamental mode field may not always be valid [46–48]. In this direction, Hirooka *et al.* [35] have reported that approximating the electrical field of the principal mode of H-MOFs with weakly guiding structures by Gaussian function brought out large errors; therefore, they proposed that Gaussian function should be replaced by hyperbolic-secant function. For the MOFs with strongly guiding structures, Gaussian function should still be used. An analytical field model for lowest-order core mode of index-guiding MOF with one-rod core was proposed by Sharma and Chauhan [49] in 2009, and they utilized the variational method to obtain the propagation constant of the mode. Ghosh *et al.* [50] also employed the variational approach for estimating the modal effective indices and the dispersion characterises of solid-core MOFs. In 2012, Zhang *et al.* [51] proposed a constructed function for approximating the mode field precisely in MOFs by using the least square error criteria. Recently, we have proposed an improved theoretical model [52] for solid-core H-MOF and utilized it for exploring the fundamental propagation characteristics of H-MOFs with different configurations. Using the improved model, we have also evaluated the optimum splicing between H-MOFs and the standard fibre [53].

In this paper, we aim to investigate the beam divergence angle by using improved theoretical model for the guided fundamental mode of one-rod core H-MOFs with different geometries. Also, we confirmed the predictions of the wavelength dependent nature of beam divergence angle by using the effective index model. For validating the simulated results we made comparison with experimental results as reported in the literature.

The article is arranged as follows: a brief review on theoretical modeling is given in Section 2, and the theoretical aspects on beam divergence are explored in Section 3. Section 4 is dedicated to present results based on theoretical investigations as the function of wavelength for one-rod core H-MOF, as well as the discussion of the differences in the results between the experimentally measured and those based on the improved field model. In Section 5 finally, conclusions are briefed.

2. Theoretical model

The fundamental modal characteristics of H-MOF in many aspects resemble to those of standard SIF due to the resemblance of light guidance mechanism [12–15]; however, differences occur as a result of intricate geometry of the porous cladding structure [11,29]. For exploring the performance of one-rod core H-MOFs, we utilized our earlier developed improved theoretical model (detailed have been reported in Ref 52). The microstructured region after the 5th ring has been modelled as a homogenous medium (as shown schematically in Fig. 1) of effective index equal to that of lowest-order cladding mode (n_{FSM}) also, known as fundamental space-filling mode (FSM) [11,54]. FSM is the principal cladding mode [54–56] for an infinitely extended cladding medium if the core is absent having the same symmetries as that of the photonic crystal itself [11,14].

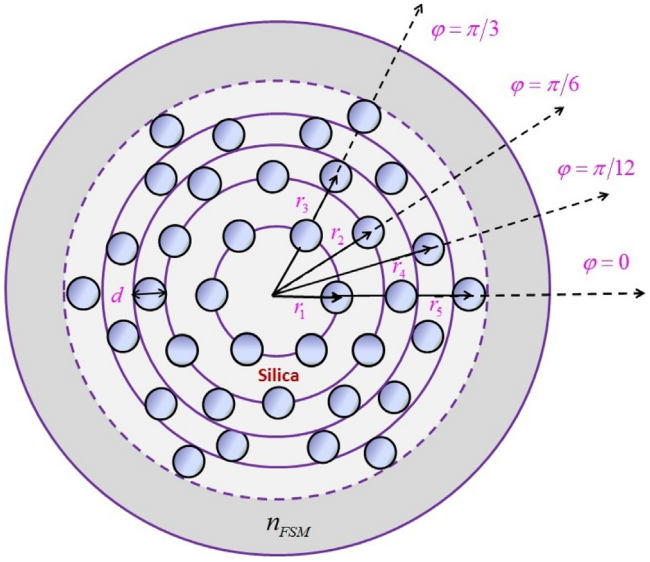

Fig. 1. Schematic diagram illustrating dielectric cross-section for one-rod core H-MOF [52].

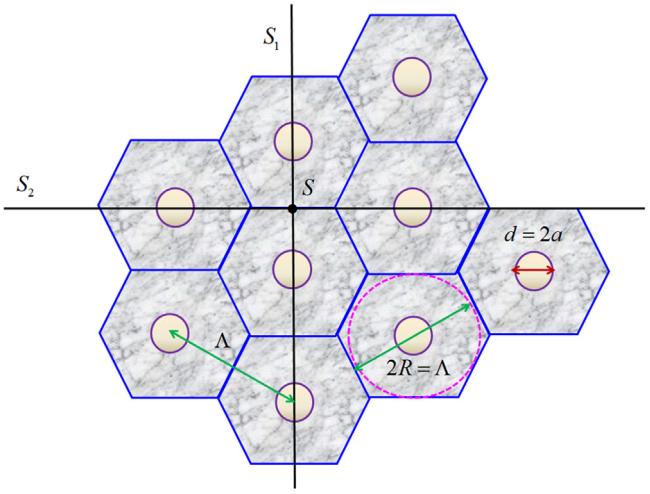

Fig. 2. MOF cladding structure (as shown schematically) with hexagonal and corresponding circular unit cell and the planes of symmetry are depicted by solid straight lines S_1 and S_2.

2.1. Principal cladding mode

The cladding effective index is a critical parameter for realizing a single-mode MOF; therefore, it should be determined with appreciable accuracy. For evaluating n_{FSM}, we have utilized weakly guiding approximation [56]. We obtained the following characteristics equation [54,55] (in terms of Bessel functions *I*, *J* and *Y*) on arresting the boundary condition:

$$wI_1(aw)(J_1(uR)Y_0(au) - Y_1(uR)J_0(au)) + uI_0(aw)(J_1(uR)Y_1(au) - Y_1(uR)J_1(au)) = 0, \quad (1)$$

where $u = \left(n_{si}^2 k_0^2 - \beta_{FSM}^2\right)^{1/2}$, $w = \left(\beta_{FSM}^2 - n_{air}^2 k_0^2\right)^{1/2}$, $a\,(= 0.5d)$ is the air-hole radius and k_0 is the free-space wave vector. The effective radius for equivalent circular unit cell (as shown schematically in Fig. 2) is denoted by $R = 0.5\Lambda$ [30,56]. $\beta_{FSM}\,(= k_0 n_{FSM})$ is the propagation constant for the FSM along the axis of crystal [54].

2.2. Principal core mode

An explicit interpretation of the modal field guided in transverse cross-section of an optical waveguide is essential for investigating its propagation characteristics. However, for the waveguide like H-MOFs with no shape core-cladding interface makes its dielectric cross-section unconventioal; therefore, it becomes cumbersome to predict the functional form of the principal mode. Approximate methods like perturbation and WKB methods [57,58] have their limitations; therefore, they are not trustworthy. Intuitively, we choose scalar variational method [59–62] to endeavour the functional configuration of the field. In order to consider the field asymmetries, we chose the following trial electric field [52,53]:

$$\Psi(r,\varphi) = \exp(-\alpha r^2) - (A\exp(-\alpha_1(r-\sigma\Lambda)^2)(1+\cos 6\varphi)) - (B\exp(-\alpha_2(r-\eta\Lambda\sqrt{3})^2)(1-\cos 6\varphi)), \quad (2)$$

where $A, \alpha, \alpha_1, \sigma, B, \alpha_2$ and η are the variables, and Λ is the pitch (detailed have been reported in Ref. 52). For assessing propagation constant for the waveguiding structure with $n^2(r,\varphi)$ as its refractive index profile, we begin with Helmholtz wave equation under weakly guiding approximation [34]:

$$\left(\frac{\partial^2}{\partial r^2} + \frac{1}{r}\frac{\partial}{\partial r} + \frac{1}{r^2}\frac{\partial^2}{\partial \varphi^2}\right)\Psi(r,\varphi) + (k_0^2 n^2(r,\varphi) - \beta^2)\Psi(r,\varphi) = 0. \quad (3)$$

We target to access the largest value for the propagation constant (using MATLAB® Optimization toolbox, for details see, e.g., Refs. 52 and 53) by using the following expression [58–61];

$$\beta^2 = \left(\int_0^{2\pi}\int_0^{\infty} n^2(r,\varphi)k_0^2|\Psi(r,\varphi)|^2 - \left(\left|\frac{\partial\Psi}{\partial r}\right|^2 + \frac{1}{r^2}\left|\frac{\partial\Psi}{\partial\varphi}\right|^2\right)ds\right) \times \left(\int_0^{2\pi}\int_0^{\infty}|\Psi(r,\varphi)|^2 ds\right)^{-1}, \quad (4)$$

where $ds\,(= rdrd\varphi)$ is the cross-sectional area. It is noteworthy that the selection of the trial field is the pivotal step for strengthen the potency and relevance of the present method [59–61].

3. Beam divergence

In traditional step-index fibres (SIFs) index difference, Δn practically remains constant with a wavelength facilitating to define the numerical aperture, *NA* in terms of core index, n_{co} by using the following expression [62,63]; $NA = \sqrt{n_{co}^2 - n_{cl}^2} = n_{co}\sqrt{2\Delta n}$; where n_{cl} is the cladding index. In one-rod core H-MOF cladding index, as well as the dispersion characteristics both can be altered by tailoring the structure of air-holes. At shorter wavelengths (i.e., when $\lambda \approx d$; where d is the air-hole diameter) cladding index is nearly close to that of background material resulting leakage of the guided mode through narrow silica bridges far away from the core [31,34]. But the same is not happen in longer wavelength regime (when λ is far greater than d and Λ). The electric field penetrates deeply into the air-holes at longer wavelengths reducing the effective index for cladding mode consequently both Δn and *NA* increases [64]. The Gaussian approximation for the principal guided core mode [34] gives the spot radius, ω_s as: $\omega_s/a_c = 1/\sqrt{\ln V}$; where the normalized frequency (or V - parameter), is given by the following expression [62,63]; $V = a_c\left(2\pi/\lambda\right)NA$; where a_c is the fibre's core radius. The Gaussian beam propagation theory announce that beam divergence angle is [33,64] $\theta_f = \lambda/\pi\omega_s$. On eliminating, ω_s, we have the following expression in terms of *NA* [33]:

$$\theta_f = NA\left(2\sqrt{\ln V}/V\right). \quad (5)$$

It can be noted that at the shorter wavelengths, *NA* is proportional to wavelength; therefore, V - parameter is virtually constant. With increase in wavelength slope of θ_f *vs.* λ will decrease as *NA* become flattened [33,62].

Table 1
Cladding parameters of the high-index core H-MOFs.

Fibre ID	Λ (μm)	d/Λ	Refs.
MOF1	2.39	0.26	[33]
MOF2	7.2	0.53	[64]

4. Simulated results and discussion

We considered two structures of high-index core H-MOFs with one-rod core in which light is guided through total internal reflection [65], and their fundamental cladding parameters are listed in Table 1. For simulation, we considered that the refractive index of background material (which is undoped fused silica) is 1.45.

The divergence measurements for traditional SIF can be based on $1/e$ of the field radius facilitated by circular symmetry of the mode [62,64]; however, the complex spatial configuration of MOF makes the mode non symmetric [33], which can be visualized from Fig. 3. The near-field (NF) profile for principal mode of H-MOFs (structural parameters are summarized in Table 1) is shown in Fig. 3 at the operating wavelength of 0.65 μm. It can be observed from Fig. 3(b) that MOF2 with larger air-holes have strongly confined modal field and it looks more circularly symmetric in contrast to mode profile of MOF1 [see Fig. 3(a)]. MOF1 with smaller air-hole diameter facilitating the leakage of field into the porous cladding with long tail extended far away from the core into the cladding. Thus, we can infer that NF-pattern for fundamental guided core mode of both fibres have circular symmetry close to their centre (indicating that the field profile can be approximated by simple Gaussian function) but it becomes more hexagonal in the wings of the field [see Fig. 3(a)]. Thus, it can be depicted from Fig. 3 that the field profile for smaller d/Λ ratio (i.e., weakly guiding structure) is evidently different that of higher d/Λ value (i.e., strongly guiding structure).

It is noteworthy that NF measurement techniques are prone to distortion and instability. Since far-field (FF) pattern is much wider; therefore, profound deploying conditions are not mandatory [66–69]; moreover, it remains unaffected if the fibre is twisted [14,15]. Therefore, it is the matter of great concern to determine the spatial FF radiation pattern for understanding and analysing the behaviour of the lowest-order core mode in single-mode fibres. Classical fibres are cylindrically symmetric; therefore, their FF-profile will be cylindrically symmetric [62] and has been extensively examined by various authors [70,71]. Contrarily, the hexagonal symmetry of one-rod core H-MOFs has significant disclosure in the radiated field pattern as explored in Refs. 69 and 72. Knight *et al.* [14] reported experimentally an MOF with hexagonal symmetry supporting a single robust guided mode and concluded that FF-pattern looks remarkably similar over the broad spectral range. The amplitude, $\rho\left(\theta\right)$ at the far-field angle, θ can be evaluated by using the well-known Fraunhoffer's diffraction formula [73]: $\rho\left(\theta\right) = C_0\int_0^{2\pi}\int_0^{\infty}\Psi(r,\varphi)\exp\left(ik_0 r\sin\theta\cos\varphi\right)rdrd\varphi$; where C_0 is a constant, and $\Psi(r,\varphi)$ is given by Eq. (2). It is noteworthy that the above integral represents 2D Fourier transform of NF-

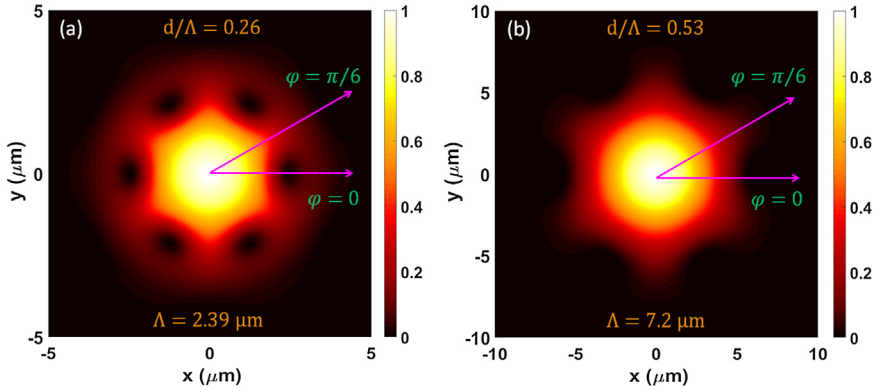

Fig. 3. The near-field profile for (a) MOF1 (with Λ =2.39 μm and d/Λ = 0.26), and (b) MOF2 (with Λ =7.2 μm and d/Λ = 0.53) at the wavelength of 0.65 μm.

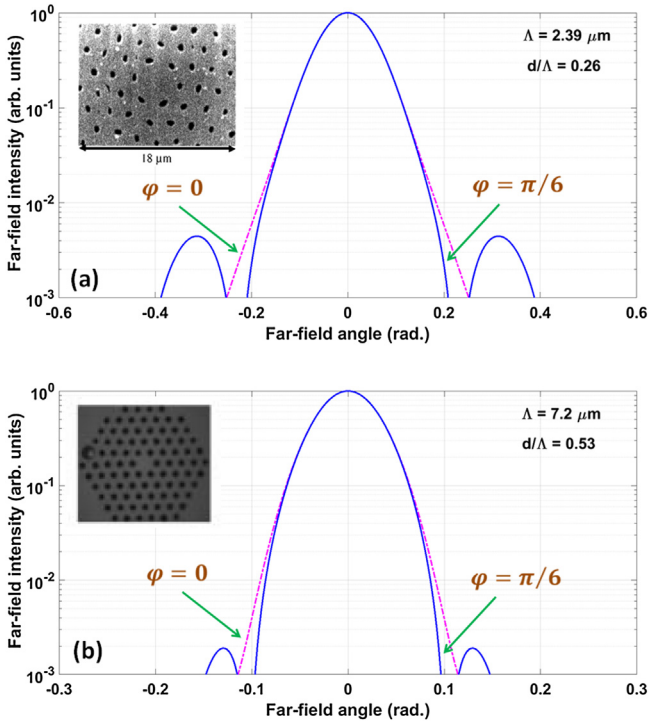

Fig. 4. Normalized far-field intensity profile for one-rod core (a) MOF1 and (b) MOF2 at the wavelength of 0.65 μm in $\varphi = 0$ (as displayed by dash-dotted line) and $\varphi = \pi/6$ (as displayed by solid line) directions (Inset depicts scanning electron micrograph (SEM) of the dielectric cross-section for MOF1 [33] and MOF2 [64]).

profile [62]. The normalized FF-intensity, i.e., $I_{FF}\left(\theta\right) = \left|\tilde{\rho}\left(\theta\right)\right|^2 = \left|\rho\left(\theta\right)/\rho(0)\right|^2$ against the far-field angles (in radians) for MOF1 (Λ =2.39 μm and d/Λ = 0.26) and MOF2 (Λ =7.2 μm and d/Λ = 0.53) at 0.65 μm in principle directions (i.e., $\varphi = 0$ and $\varphi = \pi/6$) of observation is illustrated in Fig. 4, where side lobes of substantial magnitude can be seen in $\varphi = \pi/6$ direction.

From Fig. 4, it can be illustrated that FF-intensity profile with low intensity satellite peaks is approximately Gaussian in nature; moreover, there is no remarkable departure from the Gaussian profile above $1/e^2$ level in both directions of observation. Therefore, mode profile may be assumed to be circularly symmetric (or Gaussian). Of course, we can neglect the low intensity satellite spots as observed in FF-pattern (see Fig. 4) of the mode in one-rod core H-MOFs (leading to non-Gaussian nature of field profile) [14] as they give only a minor contribution [69].

For quantifying the inherent asymmetry associated with mode profile (or to treat the axially non-symmetry associated with one-rod core H-MOF), we instinctively used the Petermann-2 spot-size, which is related to the root mean square width of FF-pattern, is defined as [74,75]:

$$\omega_{p_{II}} = \sqrt{2}\left(\left(\int_0^{2\pi}\int_0^{\infty}|\Psi(r,\varphi)|^2 r dr d\varphi\right)\left(\int_0^{2\pi}\int_0^{\infty}(d\Psi/dr)^2 r dr d\varphi\right)^{-1}\right)^{1/2}, \quad (6)$$

where $\Psi(r,\varphi)$ is given by Eq. (2). With this definition, $\omega_{p_{II}}$ remains $1/e^2$ of the intensity radius for a Gaussian beam and facilitating an elegant way to evaluate the spot-size for the non-Gaussian beam.

Koshiba and Saitoh [32] discussed the appropriateness of well-established standard fibre theories to H-MOFs by suitably formulating the V-parameter (or normalized frequency) and estimated the fundamental propagation properties through simple empirical expressions, and confirmed the rationality by comparing with experimental and numerical results. Under step-index fibre approximation (SIFA) for one-rod core H-MOF [33,76], integrals involved in Eq. (6) can be evaluated analytically in terms of Bessel functions J_0 and J_1, to facilitate the following expression [34,62]:

$$\omega_{SIFA} = \sqrt{2}\left(a_{co}\left[J_1\left(U_{eff}\right)/W_{eff}J_0\left(U_{eff}\right)\right]\right), \quad (7)$$

where $U_{eff} = \left(2\pi/\lambda\right)a_{co}\sqrt{n_{co}^2 - n_{eff}^2}$ and $W_{eff} = \left(2\pi/\lambda\right)a_{co}\sqrt{n_{eff}^2 - n_{FSM}^2}$ are the normalized transverse phase and the attenuation parameters [77], a_{co} is the effective core radius, n_{FSM} is the effective cladding index, and λ being the operating wavelength. The Gaussian approximation for one-rod core H-MOF [32], facilitate to express the modal spot-size through an empirical expression, known as Marcuse formula [62,78]:

$$\omega_M = a_{co}(0.65 + (1.619/V_{eff}^{1.5}) + (2.879/V_{eff}^{6})), \quad (8)$$

where $V_{eff} = \left(\sqrt{U_{eff}^2 + W_{eff}^2}\right)$ is the effective normalized frequency (or V_{eff} -parameter) defined for the MOFs which can be expressed as [32,77]: $V_{eff} = \left(2\pi/\lambda\right)a_{co}\sqrt{n_{co}^2 - n_{FSM}^2}$.

For establishing an analogy between H-MOF and traditional SIF, it is crucial to define the effective core radius, so that the single-mode behaviour can be explained [47]. The choice of an appropriate definition for the size of MOF's core is not obvious as there is no sharp core-cladding interface; therefore, it is arbitrary up to the certain extent [56]. As a common practice, when formulating V_{eff} -parameter for high-index core H-MOF, one may choose any transverse dimension for the core radius, and it was first set to a value of $a_{co} = \Lambda$ [8,15], which is roughly the radius of local lattice defect site. Gander *et al.* [33] adopted the formulation of effective V-value to solid-core H-MOF under SIFA with $a_{co} = \Lambda$.

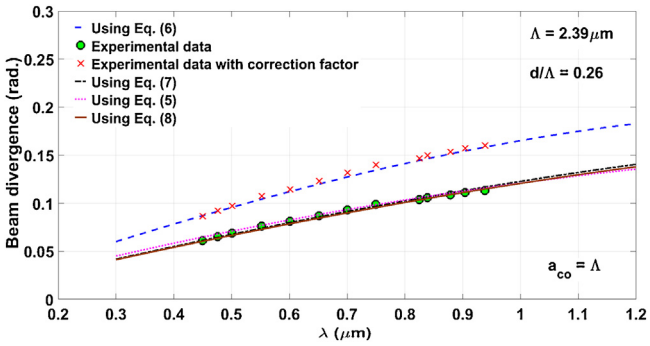

Fig. 5. Beam divergence against wavelength for an MOF1 with Λ =2.39 μm and normalized air-hole diameter ratio of d/Λ = 0.26.

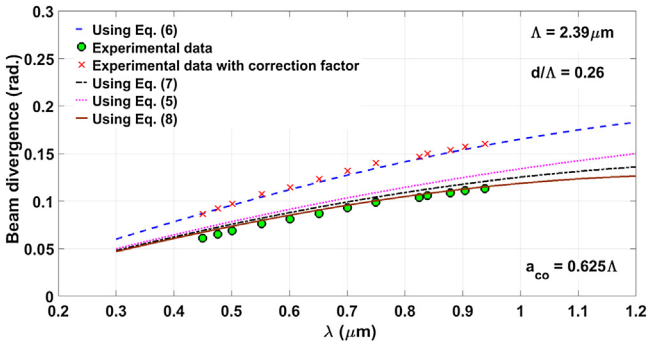

Fig. 6. Spectral dependence of beam divergence (rad.) for high-index core triangular MOF1 with pitch of 2.39 μm and d/Λ = 0.26.

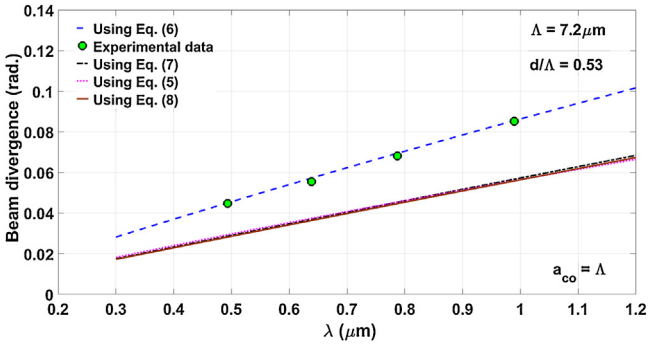

Fig. 7. Beam divergence (rad.) against wavelength (μm) for MOF2 with pitch, Λ of 7.2 μm and relative air-hole diameter ratio, d/Λ of 0.53.

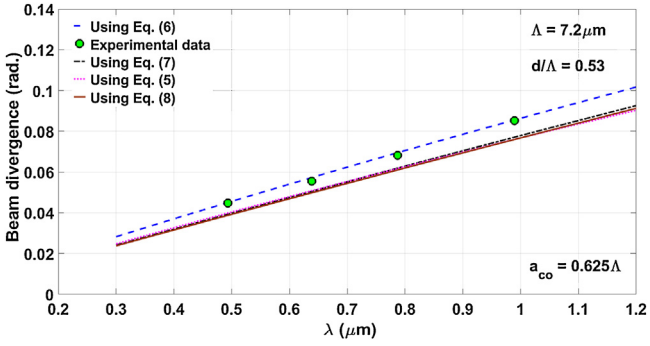

Fig. 8. Variation of beam divergence for MOF2 with Λ =7.2 μm and d/Λ = 0.53.

To provide the theoretical predictions in accordance with experiments under this choice of core radius, the cut-off frequency of the second mode is set at a value higher than the usual value of 2.405, as used for standard SIF. However, with further calculations including comparisons with the results of other methods, Brechet *et al.* [79] investigated that the propagation constant of the mode of MOFs are close to those of a SIF if the effective core radius is approximated by 0.64Λ. Later on, Birks *et al.* [80] reported the optimized value for the effective core radius, $a_{co} = 0.625\Lambda$, which is the widely accepted choice for a_{co} under SIFA for one-rod core H-MOF [81].

The variation of beam divergence against wavelength (ranging from 0.2 μm to 1.2 μm) for the MOF1 is illustrated in Fig. 5; where we have shown the results obtained from Eq. (6), [which is based on Petermann-2 spot-size (for details, see appendix **A**)] using the improved model. Theoretical results obtained from Eq. (5) (based on Gaussian beam propagation theory, as displayed by dotted line), Eq. (7) (Pertermann-2 spot-size under SIFA, as shown by dash-dotted line) and Eq. (8) (based on Marcuse formula, as displayed by solid line), for one-rod core H-MOF with $a_{co} = \Lambda$ [8,15] also have been included. We have incorporated the experimental data (as displayed by solid circle), quoted from Ref. [33], which are matching well to those obtained from Eqs. (5), (7), and (8). Hence, justifying the choice of $a_{co} = \Lambda$, this is indeed an obvious choice to define the effective core radius for an MOF.

In Fig. 6, results are shown for the same fibre under SIFA with the choice of $a_{co} = 0.625\Lambda$. Appreciable spreading among the results based on Eqs. (5), (7), and (8) can be observed (see Fig. 6) implying that SIF approximation with $a_{co} = 0.625\Lambda$ for MOF1 does not hold well. We have considered both definitions of core radii for evaluating the results (see Fig. 5 and Fig. 6) based on Eqs. (5) and (7), indicating that they are depending upon the choice of the value to be used as a_{co}. Therefore, it can be argued that these methods will provide less accurate results for evaluating the divergence angle, θ_f.

It is noticeable that the results obtained from Eq. (8) (which are based on Marcuse formula and as shown by solid line in Fig. 5 and Fig. 6 are matching well to experimental data points [33], for the entire range of wavelength indicating that they are independent of the choice of a_{co}. Therefore, it can be argued that Marcuse formula will be more trustworthy for evaluating θ_f as compared to those based on Eqs. (5) and (7).

Theoretical results based on Eq. (6) as shown by dashed line in Fig. 5 and Fig. 6 are far away from the experimental data points (as shown by solid circles). This difference can be compensated, if we multiply the experimental data points by a factor of $\sqrt{2}$, as a correction factor. The results of experimental data with a correction factor (as shown by cross marks) for MOF1 is shown in Fig. 5 and Fig. 6, which are good in agreement to our theoretical results, suggesting that the procedure used in Ref. 33, for evaluating the beam divergence may have inadvertently introduced a factor of $\sqrt{2}$ in its definition of the divergence. Also, we would like to emphasized that there is experimental variation in air-hole size [33], resulting in some sort of uncertainty in the calculated values of θ_f. It should be noted that the theoretical model cannot account for the clear non-circularity in the air-holes diameter, which is apparent from the SEM image [see inset of Fig. 4(a)].

In Fig. 7, we have illustrated beam divergence for MOF2 as a function of wavelength. The results obtained from Eq. (5) (as illustrated by dotted line), Eq. (7) (as illustrated by dash-dotted line), and Eq. (8) (as illustrated by solid line), which are based on SIFA used for high-index core H-MOF with $a_{co} = \Lambda$ [8,15], are also included. For checking the accuracy of results (obtained from Eq. (6) as illustrated by dashed line, evaluated by using improved theoretical model) experimental data [33] (as illustrated by solid circles) has been included.

On choosing $a_{co} = 0.625\Lambda$ [80,81], which is the optimized core radius for high-index core H-MOF under SIFA, the results for MOF2 fibre (see Fig. 8) are following the same trend but still they are not matching to experimental data. The results based on Eqs. (5),

(7), and (8) for MOF2 fibre (see Fig. 7 and Fig. 8) are overlapping, suggesting that these methods will provide nearly identical values of θ_f under SIFA. There is an ambiguity (see Fig. 7 and 8) in matching of the results based on SIFA to the experimental data; therefore, demanding a more accurate definition for the choice of a_{co}.

Results based on Eq. (6), evaluated by using the modal field as given by Eq. (2) are coherent to experimental data (see Fig. 7 and Fig. 8) for one-rod core MOF2 fibre [64]. Thus, we can infer that our improved field model is independent of the way of defining and choosing the effective core radius.

At this point, we can argue that the qualitative predictions of the theory that the beam divergence is proportional to wavelength for shorter wavelength realm contrarily to what happens at longer wavelengths, are well assisted by the results obtained from using the improved theoretical model. Also, we would like to emphasize that the model is based on weakly guiding approximation despite it facilitate the results which are coherent to those based on experimental measurements.

5. Conclusions

We utilized the extended form of our theoretical model for two different configurations of one-rod core H-MOFs, and examined the wavelength dependence of beam divergence for H-MOFs over the wavelength range of 0.2–1.2 μm. Our theoretical results are coherent to experimental data for MOF2 fibre and independent of the choice of effective core radius.

For MOF1 fibre our result follows the same trend as reported in literature [33], and they are coherent to experimental data only after corrected by a factor of $\sqrt{2}$, indicating errors in the measurement of data.

We are assured that our theoretical model can furnish an efficient route to evaluate the divergence angle with adequate accuracy, which facilities to estimate the numerical aperture possessing the potential impact in the domain of fiber laser based applications. In spite of that our analytical approach can be employed for tuning the numerical aperture with wavelength and, thus, alleviating the necessity of fiber post-processing.

Author statement

Development of methodology, creation of model, designing and implementation of computer code/supporting algorithms, creation and editing of manuscript is done by Dr. Dinesh Kumar Sharma. Oversight and leadership responsibility for research activity planning and execution, and acquisition of financial support to this publication is being supported by Dr. Saurabh Mani Tripathi.

Acknowledgements

D.K. Sharma is sincerely grateful to IIT Kanpur, Kanpur (U.P) India for providing the Institute Post-doctoral Fellowship (PDF-102). The author wishes to thank Prof. Anurag Sharma, IIT Delhi for his fruitful conversation and Dr. S.M. Tripathi for his kind encouragement.

Appendix A. Petermann-2 spot-size

$$\omega_{p_{II}} = \sqrt{2}\left(\left(\int_0^{2\pi}\int_0^{\infty}\left|\Psi(r,\varphi)\right|^2 r dr d\varphi\right)\left(\int_0^{2\pi}\int_0^{\infty}\left(d\Psi/dr\right)^2 r dr d\varphi\right)^{-1}\right)^{1/2}$$
$$= \sqrt{2}\left[\frac{I_1}{I_2}\right]^{1/2} \tag{A1}$$

where $\Psi(r,\varphi)$ represents the scalar near-field as given by Eq. (2).

$$\left|\Psi(r,\varphi)\right|^2 = e^{-2\alpha r^2} + A^2 e^{-2\alpha_1(r-\sigma\Lambda)^2}(1+\cos 6\varphi)^2$$
$$+B^2 e^{-2\alpha_2\left(r-\eta\sqrt{3}\Lambda\right)^2}(1-\cos 6\varphi)^2$$
$$-2Ae^{-\alpha r^2-\alpha_1(r-\sigma\Lambda)^2}(1+\cos 6\varphi) + 2ABe^{-\alpha_1(r-\sigma\Lambda)^2-\alpha_2\left(r-\eta\sqrt{3}\Lambda\right)^2}$$
$$(1+\cos 6\varphi)(1-\cos 6\varphi)$$
$$-2Be^{-\alpha r^2-\alpha_2\left(r-\eta\sqrt{3}\Lambda\right)^2}(1-\cos 6\varphi) \tag{A2}$$

We can express integral, I_1, as the sum of six integrals which are given below:

$$I_1 = \int_0^{2\pi}\int_0^{\infty}\left|\Psi(r,\varphi)\right|^2 r dr d\varphi = I_{11}+I_{12}+I_{13}+I_{14}+I_{15}+I_{16}, \tag{A3}$$

where,

$$I_{11} = \int_0^{2\pi} d\varphi \int_0^{\infty} e^{-2\alpha r^2} r dr = 2\pi\int_0^{\infty} e^{-2\alpha r^2} r dr$$

$$I_{12} = \int_0^{2\pi}(1+\cos 6\varphi)^2 d\varphi \int_0^{\infty} A^2 e^{-2\alpha_1(r-\sigma\Lambda)^2} r dr$$
$$= 3\pi A^2\int_0^{\infty} e^{-2\alpha_1(r-\sigma\Lambda)^2} r dr$$

$$I_{13} = \int_0^{2\pi}(1-\cos 6\varphi)^2 d\varphi \int_0^{\infty} B^2 e^{-2\alpha_2\left(r-\eta\sqrt{3}\Lambda\right)^2} r dr$$
$$= 3\pi B^2\int_0^{\infty} e^{-2\alpha_2\left(r-\eta\sqrt{3}\Lambda\right)^2} r dr$$

$$I_{14} = -\int_0^{2\pi}(1+\cos 6\varphi)\, d\varphi \int_0^{\infty} 2Ae^{-\alpha r^2-\alpha_1(r-\sigma\Lambda)^2} r dr$$
$$= -4\pi A\int_0^{\infty} e^{-\alpha r^2-\alpha_1(r-\sigma\Lambda)^2} r dr$$

$$I_{15} = -\int_0^{2\pi}(1-\cos 6\varphi)\, d\varphi \int_0^{\infty} 2Be^{-\alpha r^2-\alpha_2\left(r-\eta\sqrt{3}\Lambda\right)^2} r dr$$
$$= -4\pi B\int_0^{\infty} e^{-\alpha r^2-\alpha_2\left(r-\eta\sqrt{3}\Lambda\right)^2} r dr$$

$$I_{16} = \int_0^{2\pi}(1+\cos 6\varphi)(1-\cos 6\varphi)$$
$$d\varphi\int_0^{\infty} 2ABe^{-\alpha_1(r-\sigma\Lambda)^2-\alpha_2\left(r-\eta\sqrt{3}\Lambda\right)^2} r dr$$
$$= 2\pi AB\int_0^{\infty} e^{-\alpha_1(r-\sigma\Lambda)^2-\alpha_2\left(r-\eta\sqrt{3}\Lambda\right)^2} r dr.$$

Integral, I_2 can be expressed as the sum of six integrals, which are given below;

$$I_{21} = \int_0^{2\pi}\int_0^{\infty}\left|\frac{\partial\Psi}{\partial r}\right|^2 r dr d\varphi = I_{21}+I_{22}+I_{23}+I_{24}+I_{25}+I_{26}, \tag{A4}$$

where,

$$I_{21} = \int_0^{2\pi} d\varphi \int_0^{\infty} 4\alpha^2 e^{-2\alpha r^2} r^2 r dr = 8\pi\alpha^2 \int_0^{\infty} e^{-2\alpha r^2} r^3 dr$$

$$I_{22} = \int_0^{2\pi} (1+\cos 6\varphi)^2 d\varphi \int_0^{\infty} 4A^2\alpha_1^2 (r-\sigma\Lambda)^2 e^{-2\alpha_1 (r-\sigma\Lambda)^2} r dr$$
$$= 12\pi A^2\alpha_1^2 \int_0^{\infty} (r-\sigma\Lambda)^2 e^{-2\alpha_1 (r-\sigma\Lambda)^2} r dr$$

$$I_{23} = -\int_0^{2\pi} (1+\cos 6\varphi)\, d\varphi \int_0^{\infty} 8A\alpha\alpha_1 (r-\sigma\Lambda)\, e^{-\alpha r^2 - \alpha_1 (r-\sigma\Lambda)^2} r^2 dr$$
$$= -16\pi A\alpha\alpha_1 \int_0^{\infty} (r-\sigma\Lambda)\, e^{-\alpha r^2 - \alpha_1 (r-\sigma\Lambda)^2} r^2 dr$$

$$I_{24} = \int_0^{2\pi} (1-\cos 6\varphi)^2 d\varphi \int_0^{\infty} 4B^2\alpha_2^2 \left(r-\eta\sqrt{3}\Lambda\right)^2 e^{-2\alpha_2 \left(r-\eta\sqrt{3}\Lambda\right)^2} r dr$$
$$= 12\pi B^2\alpha_2^2 \int_0^{\infty} \left(r-\eta\sqrt{3}\Lambda\right)^2 e^{-2\alpha_2 \left(r-\eta\sqrt{3}\Lambda\right)^2} r dr$$

$$I_{25} = -\int_0^{2\pi} (1-\cos 6\varphi)\, d\varphi \int_0^{\infty} 8B\alpha\alpha_2 \left(r-\eta\sqrt{3}\Lambda\right)$$
$$e^{-\alpha r^2 - \alpha_2 \left(r-\eta\sqrt{3}\Lambda\right)^2} r^2 dr$$
$$= -16\pi B\alpha\alpha_2 \int_0^{\infty} \left(r-\eta\sqrt{3}\Lambda\right) e^{-\alpha r^2 - \alpha_2 \left(r-\eta\sqrt{3}\Lambda\right)^2} r^2 dr$$

$$I_{26} = \int_0^{2\pi} (1-\cos 6\varphi)(1+\cos 6\varphi)$$
$$d\varphi \int_0^{\infty} 8AB\alpha_1\alpha_2 (r-\sigma\Lambda)(r-\eta\sqrt{3}\Lambda) e^{-\alpha_1 (r-\sigma\Lambda)^2 - \alpha_2 (r-\eta\sqrt{3}\Lambda)^2} r dr$$
$$= 8\pi AB\alpha_1\alpha_2 \int_0^{\infty} (r-\sigma\Lambda)(r-\eta\sqrt{3}\Lambda) e^{-\alpha_1 (r-\sigma\Lambda)^2 - \alpha_2 (r-\eta\sqrt{3}\Lambda)^2} r dr.$$

References

[1] J. Arriaga, J.C. Knight, P.St.J. Russell, Modelling the propagation of light in photonic crystal fibres, Phys. D 189 (2004) 100–106.
[2] J.C. Knight, T.A. Birks, R.F. Cregan, P.St.J. Russell, J.-P. de Sandro, Photonic crystals as optical fibres - physics and applications, Opt. Mater. 11 (1999) 143–151.
[3] E. Yablonovitch, Photonic band-gap structures, J. Opt. Soc. Am. B 10 (1993) 283–295.
[4] T.F. Krauss, R.M. De La Rue, S. Brandt, Two-dimensional photonic band gap structures operating at near-infrared wavelengths, Nature 383 (1996) 699–702.
[5] A. Mekis, J.C. Chen, I. Kurland, S.H. Fan, P.R. Villeneuve, J.D. Joannopoulos, High transmission through sharp bends in photonic crystal waveguides, Phys. Rev. Lett. 77 (1996) 3787–3790.
[6] D.M. Atkin, P.St.J. Russell, T.A. Birks, P.J. Roberts, Photonic band structure of guided Bloch modes in high index films fully etched through with periodic microstructure, J. Mod. Opt. 43 (1996) 1035–1053.
[7] T.A. Birks, P.J. Roberts, P.St.J. Russell, D.M. Atkin, T.J. Shepherd, Full 2-D photonic band gaps in silica/air structures, Electron. Lett. 31 (1995) 1941–1943.
[8] J.C. Knight, T.A. Birks, P.St.J. Russell, J.P. de Sandro, Properties of photonic crystal fiber and the effective index model, J. Opt. Soc. Am. A 15 (1998) 748–752.
[9] P.L. Gourley, J.R. Wendt, G.A. Vawter, T.W. Brennan, B.E. Hammons, Optical properties of two-dimensional photonic lattices fabricated as honeycomb nanostructures in compound semiconductors, Appl. Phys. Lett. 64 (1994) 687–689.
[10] R. Tonucci, B.L. Justus, A.J. Campillo, C.E. Ford, Nanochannel array glass, Science 258 (1992) 783–785.
[11] P.St.J. Russell, Photonic-crystal fibers, J. Lightwave Technol. 24 (2006) 4729–4749.
[12] P.St.J. Russell, Photonic crystal fibers, Science 299 (2003) 358–362.
[13] J.C. Knight, Photonic crystal fibers, Nature 424 (2003) 847–851.
[14] J.C. Knight, T.A. Birks, P.St.J. Russell, D.M. Atkin, All-silica single-mode optical fiber with photonic crystal cladding, Opt. Lett. 21 (1996) 1547–1549, see also errata Opt. Lett., 22, 484-485 (1997).
[15] T.A. Birks, J.C. Knight, P.St.J. Russell, Endlessly single-mode photonic crystal fiber, Opt. Lett. 22 (1997) 961–963.
[16] W.H. Reeves, J.C. Knight, P.St.J. Russell, P.J. Roberts, Demonstration of ultra-flattened dispersion in photonic crystal fibers, Opt. Exp 10 (2002) 609–613.
[17] T.M. Monro, D.J. Richardson, N.G.R. Broderick, P.J. Bennett, Holey optical fibers: an efficient modal model, J. Lightwave Technol. 17 (1999) 1093–1102.
[18] T.M. Monro, D.J. Richardson, N.G.R. Broderick, P.J. Bennett, Modelling large air fraction holey optical fibers, J. Lightwave Technol. 18 (2000) 50–56.
[19] D. Mogilevtsev, T.A. Birks, P.St.J. Russell, Group-velocity dispersion in photonic crystal fiber, Opt. Lett. 23 (1998) 1662–1664.
[20] J.C. Knight, J. Broeng, T.A. Birks, P.St.J. Russell, Photonic band gap guidance in optical fibers, Science 282 (1998) 1476–1478.
[21] T.M. Monro, P.J. Bennett, N.G.R. Broderick, D.J. Richardson, Holey fibers with random cladding distributions, Opt. Lett. 25 (2000) 206–208.
[22] W.J. Wadsworth, J.C. Knight, W.H. Reeves, P.St.J. Russell, J. Arriage, Yb^{3+}-doped photonic crystal fiber laser, Electron. Lett. 36 (2000) 1452–1454.
[23] K. Furusawa, T.M. Monro, P. Petropoulos, D.J. Richardson, Mode locked laser based on ytterbium doped holey fiber, Electron. Lett. 37 (2001) 560–561.
[24] T.M. Monro, Y.D. West, D.W. Hewak, N.G.R. Broderick, D.J. Richardson, Chalcogenide holey fibers, Electron. Lett. 36 (2000) 1998–2000.
[25] M.A. van Eijkelenborg, M.C.J. Large, A. Argyros, J. Zagari, S. Manos, N. Issa, I. Bassett, S. Fleming, R.C. McPhedran, C.M. de Sterke, N.A.P. Nicorovici, Microstructured polymer optical fiber, Opt. Exp. 9 (2001) 319–327.
[26] T.M. Monro, D.J. Richardson, P.J. Bennett, Developing holey fibers for evanescent field devices, Electron. Lett. 35 (1999) 1188–1189.
[27] Y.L. Hoo, W. Jin, H.L. Ho, D.N. Wang, Evanescent-wave gas sensing using microstructure fiber, Opt. Eng. 41 (2002) 8–9.
[28] S. Kim, Y. Jung, K. Oh, J. Kobelke, K. Schuster, J. Kirchhof, Defect and lattice structure for air-silica index-guiding holey fibres, Opt. Lett. 31 (2006) 164–166.
[29] T.M. Monro, H. Ebendorff-Heidepriem, Progress in microstructured optical fibers, Annu. Rev. Mater. Res. 36 (2006) 467–495.
[30] J. Broeng, D. Mogilevstev, S.E. Barkou, A. Bjarklev, Photonic crystal fibers: a new class of optical waveguides, Opt. Fiber Technol. 5 (1999) 305–330.
[31] D. Gloge, Weakly guiding fibres, Appl. Opt. 10 (1971) 2252–2258.
[32] M. Koshiba, K. Saitoh, Applicability of classical optical fibre theories to holey fibres, Opt. Lett. 29 (2004) 1739–1741.
[33] M.J. Gander, R. McBride, J.D.C. Jones, T.A. Birks, J.C. Knight, P.St.J. Russell, P.M. Blanchard, J.G. Burnett, A.H. Greenaway, Measurement of the wavelength dependence of beam divergence for photonic crystal fiber, Opt. Lett. 24 (1999) 1017–1019.
[34] A.W. Snyder, J.D. Love, Optical Waveguide Theory, Chapman & Hall, London, 1983.
[35] T. Hirooka, Y. Hori, M. Nakazawa, Gaussian and Sech approximations of mode field profiles in photonic crystal fibres, IEEE Photonics Technol. Lett. 16 (2004) 1071–1073.
[36] R.E. Wagner, W.J. Tomlinson, Coupling efficiency of optics in single-mode fibre components, Appl. Opt. 21 (1982) 2671–2687.
[37] C. Ruilier, F. Cassaing, Coupling of large telescope and single mode waveguides: application to stellar interferometry, J. Opt. Soc. Am. A 18 (2001) 143–149.
[38] O. Wallner, P.J. Winzer, W.R. Leeb, Alignment tolerances for plane-wave to single-mode fibre coupling and their mitigation by use of pigtailed collimators, Appl. Opt. 41 (2002) 637–643.
[39] Y. Dikmelik, F.M. Davidson, Fibre-coupling efficiency for free space optical communication through atmospheric turbulence, Appl. Opt. 44 (2005) 4946–4952.
[40] M. Toyoshima, Maximum fibre coupling efficiency and optimum beam size in the presence of random angular jitter for free-space laser systems and their applications, J. Opt. Soc. Am. A 23 (2006) 2246–2250.
[41] J. Ma, F. Zhao, L. Tan, S. Yu, Q. Han, Plane wave coupling into single-mode fibre in the presence of random angular jitter, Appl. Opt. 48 (2009) 5184–5189.
[42] C. Chen, H. Yang, H. Wang, S. Tong, Y. Lou, Coupling plane wave received by an annular aperture into a single-mode fibre in the presence of atmospheric turbulence, Appl. Opt. 50 (2011) 307–312.
[43] J.C.W. Corbett, J.R. Allington-Smith, Coupling starlight into single-mode photonic crystal fibre using a field lens, Opt. Express 13 (2005) 6527–6540.
[44] J. Corbett, A. Dabirian, T. Butterley, N.A. Mortensen, J.R. Allington-Smith, The coupling performance of photonic crystal fibres in fibre stellar interferometry, Mon. Not. R. Astron. Soc. 368 (2006) 203–210.
[45] J.C.W. Corbett, T.J. Morris, J.R. Allington-Smith, Tip-tilt requirements for coupling starlight into single-mode photonic crystal fibres using a lenslet: a first analysis, New Astron. Rev. 49 (2006) 675–680.
[46] M. Koshiba, K. Saitoh, Structural dependence of effective area and mode field diameter for holey fibres, Opt. Exp. 11 (2003) 1746–1756.
[47] N.A. Mortensen, J.R. Folkenberg, M.D. Nielsen, K.P. Hansen, Modal cut-off and the V parameter in photonic crystal fibres, Opt. Lett. 28 (2003) 1879–1881.
[48] J.R. Folkenberg, N.A. Mortensen, K.P. Hansen, T.P. Hansen, H.R. Simonsen, C. Jakobsen, Experimental investigation of cut off phenomena in nonlinear photonic crystal fibres, Opt. Lett. 28 (2003) 1882–1884.
[49] A. Sharma, H. Chauhan, A new analytical model for the field of microstructured optical fibres, Opt. Quant. Electron. 41 (2009) 235–242.

[50] D. Ghosh, S. Roy, S.K. Bhadra, Determination of modal effective indices and dispersion of microstructured fibres with different configurations: a variational approach, J. Mod. Opt. 57 (2010) 607–620.
[51] L. Zhang, Z. Wu, S. Gao, M. Cui, Study of a constructed function for approximating mode field in photonic crystal fibres, Opt. Eng. 51 (2012) 065003-1 –-065003-11.
[52] D.K. Sharma, A. Sharma, Improved analytical model for the field of index-guiding microstructured optical fibers, Opt. Commun. 366 (2016) 127–135.
[53] D.K. Sharma, A. Sharma, S.M. Tripathi, Optimum splicing of high-index core microstructured optical fibers and traditional single-mode fibers using improved field model, Opt. Laser Technol. 109 (2019) 157–167.
[54] Z. Zhu, T.G. Brown, Analysis of the space filling modes of photonic crystal fibres, Opt. Exp. 8 (2001) 547–554.
[55] Y. Li, C. Wang, Y. Chen, M. Hu, B. Liu, L. Chai, Solution of the fundamental space-filling mode of photonic crystal fibers: numerical method versus analytical approaches, Appl. Phys. B 85 (2006) 597–601.
[56] Y.-F. Li, C.-Y. Wang, M.-L. Hu, A fully vectorial effective index method for photonic crystal fibres: application to dispersion calculation, Opt. Commun. 238 (2004) 29–33.
[57] A. Sharma, Optimal variational method for rectangular and channel waveguides, in: Guided Wave Optics; Selected Topics, Viva Books, New Delhi, 2005.
[58] A. Ghatak, S. Lokanathan, Quantum Mechanics: Theory and Applications, Macmillan, New Delhi, 1999.
[59] A. Sharma, S.I. Hosain, A.K. Ghatak, The fundamental mode of graded-index fibers: simple and accurate variational methods, Opt. Quantum Electron. 14 (1982) 7–15.
[60] A. Sharma, J.-P. Meunier, On the scalar modal analysis of optical waveguides using approximate methods, Opt. Commun. 281 (2008) 592–599.
[61] A. Sharma, A.K. Ghatak, A variational analysis of single mode graded-index fibers, Opt. Commun. 36 (1981) 22–24.
[62] A. Ghatak, K. Thyagarajan, Introduction to Fiber Optics, Cambridge University Press, Cambridge, 1998.
[63] A. Ghatak, K. Thyagarajan, Optical Electronics, Cambridge University Press, Cambridge, 1989.
[64] N.A. Mortensen, J.R. Folken, P.M.W. Skovgaard, J. Broeng, Numerical aperture of single-mode photonic crystal fibres, IEEE Photonics Technol. Lett. 14 (2002) 1094–1096.
[65] J.M. Lazaro, A. Cobo, J.M. Lopez-Higuera, Effective index and mode width sensitivities to opto-geometrical parameters on index-guided photonic crystal fibres, IEEE Photonics Technol. Lett. 20 (2008) 205–207.
[66] M. Artiglia, M. Calzavara, P.Di Vita, A. Sharma, A new procedure for analysis of single-mode-fiber far-field data, Fiber Integr. Opt. 9 (1989) 37–42.
[67] F. Villuendas, F. Calvo, J.B. Marques, Measurement of mode field radius in axially non symmetrical single-mode fibres with arbitrary power distribution, Opt. Lett. 12 (1987) 941–943.
[68] M. Young, Mode-field diameter of single-mode optical fibre by far-field scanning, App. Opt. 37 (1998) 5605–5619.
[69] N.A. Mortensen, J.R. Folkenberg, Near-field to far-field transition of photonic crystal fibers: symmetries and interference phenomena, Opt. Exp. 10 (2002) 475–481.
[70] A.C. Boucouvalas, Use of far-field radiation pattern to characterize single-mode symmetric slab waveguides, Electron. Lett. 19 (1983) 120–121.
[71] W.A. Gambling, D.N. Payne, H. Matsumura, R.B. Dyott, Determination of core diameter and refractive-index difference of single-mode fibres by observation of the far-field pattern, Microwaves Opt. Acoustics 1 (1976) 13–17.
[72] A. Dabirian, M. Akbari, N.A. Mortensen, The radiated fields of the fundamental mode of photonic crystal fibres, Opt. Exp. 13 (2005) 3999–4004.
[73] B.E.A. Saleh, M.C. Teich, Fundamentals of Photonics, John Wiley & Sons, New Jersey, 2007.
[74] M. Artiglia, G. Coppa, P. Di Vita, M. Potenza, A. Sharma, Mode field diameter measurements in single-mode optical fibres, J. Lightwave Technol. 7 (1989) 1139–1152.
[75] C. Pask, Physical interpretation of Petermann's strange spot size for single-mode fibers, Electron. Lett. 20 (1984) 144–145.
[76] K. Saitoh, M. Koshiba, Numerical modelling of photonic crystal fibres, J. Lightwave Technol. 23 (2005) 3580–3590.
[77] K. Saitoh, M. Koshiba, Empirical relations for simple design of photonic crystal fibres, Opt. Exp. 13 (2004) 267–274.
[78] D. Marcuse, Loss analysis of single-mode fibre splices, Bell Syst. Tech. J. 56 (1977) 703–718.
[79] F. Brechet, J. Marcou, D. Pagnoux, P. Roy, Complete analysis of the characteristics of propagation into photonic crystal fibres by the finite element method, Opt. Fiber Technol. 6 (2000) 181–191.
[80] T.A. Birks, D. Mogilevtsev, J.C. Knight, P.St.J. Russell, J. Broeng, P.J. Roberts, J.A. West, D.C. Allan, J.C. Fajardo, The analogy between photonic crystal fibres and step index fibres, in: Technical Digest of the Optical Fibre Communication Conference, 1999, and the International Conference on Integrated Optics and Optical Fibre Communication, OFC/IOOC' 99, IEEE Conf. Proc., 1999, 114–116.
[81] Y. Li, Y. Yao, M. Hu, L. Chai, C. Wang, Improved fully vectorial effective index method for photonic crystal fibres: evaluation and enhancement, Appl. Opt. 47 (2008) 399–406.